J Mater Sci: Mater Electron (2017) 28:18404–18417
DOI 10.1007/s10854-017-7787-4

Effect of electron-deficient linkers on the physical and photovoltaic properties of dithienopyrrole-based organic dyes

Sunil Kumar[1] · K. R. Justin Thomas[1] · Chun-Ting Li[2] · Kuo-Chuan Ho[2]

Received: 30 May 2017 / Accepted: 22 August 2017 / Published online: 30 August 2017

Abstract Organic sensitizers containing dithienopyrrole donor, benzotriazole or quinoxaline in the conjugation pathway, and cyanoacrylic acid acceptor featured in a donor–acceptor-π–acceptor configuration are reported. The effect of the nature of different conjugating bridges on photophysical, electrochemical and photovoltaic properties was systematically evaluated. The incorporation auxiliary acceptors broadened the absorption spectra and modulated the excited state energy levels. The DFT calculation unraveled a significant overlap of HOMO and LUMO orbitals in benzotriazole-containing dyes and the charge transfer character for the longer wavelength absorption. Among the dyes, a dye containing benzotriazole and thiophene in the conjugation pathway exhibited highest power conversion efficiency attributable to efficient electron injection and pronounced inhibition of electron recombination.

1 Introduction

Dye sensitized solar cell [1] (DSSC) is one of promising technology for tapping solar energy as it enjoys benefits such as low cost, facile fabrication procedure and ready availability of materials in a relatively pure form required for use. In DSSC, a sensitizer is a key element which harvests the photons of sunlight to pump the electrons from lower to higher energy states before dumping into the inorganic semiconductors [1–4]. Currently, immense attention is paid for molecular engineering of sensitizers to enhance their light harvesting ability in the red and near-IR region of sunlight and better conversion of photons into electricity [5–7]. Continuous efforts have led to progress to the extent of realizing metal-containing dyes such as ruthenium–polypyridyl [8] complexes with 11.5% power conversion efficiency (PCE), and zinc-porphyrin [9] dyes achieving PCE as high as13.0%. But, low abundance and high cost of ruthenium metal, and complicated synthesis and purification of zinc porphyrin dyes limit their widespread application. On the other hand, metal free organic dyes displayed huge potential due to their easy and low cost synthesis from wide range of raw materials [2–7]. Moreover, recently organic dyes have been demonstrated to give PCE surpassing 12.5% without the use of any additive [10].

Organic dyes usually feature a D–π–A molecular configuration which contains an electron-rich donor (D), electron-deficient acceptor (A) and a π-conjugation linker (π) [11–13]. Many attempts have been made to modify the structural elements of organic dyes in an effort to optimize the light-harvesting properties. Zhu et al. incorporated an auxiliary acceptor (A_1) and extended the configuration as, D–A_1–π–A [14]. The incorporation of auxiliary acceptors is found to be favorable for improving the photophysical, electrochemical and photovoltaic properties along with photo and thermal stabilities of the dyes [15, 16]. Commonly, auxiliary acceptors such as benzothiadiazole (BTD) [17–19], benzotriazole (BTZ) [20–22] quinoxaline (Qx) [23, 24], diketopyrrolopyrrole (DPP) [25, 26], benzoxadiazole [27, 28], etc. have been extensively used in D–A_1–π–A configuration of the dyes. Moreover, record efficiency >12.0% was achieved from

Electronic supplementary material The online version of this article (doi:10.1007/s10854-017-7787-4) contains supplementary material, which is available to authorized users.

✉ K. R. Justin Thomas
krjt8fcy@iitr.ac.in

[1] Organic Materials Laboratory, Department of Chemistry, Indian Institute of Technology Roorkee, Roorkee, India

[2] Department of Chemical Engineering, National Taiwan University, Taipei 10617, Taiwan, ROC

the D–A_1–π–A motif dyes by utilizing benzothiadiazole as auxiliary acceptor and *N*-annulated indenoperylene [10] or *N*-annulated thienocyclopentaperylene [19] as donor.

Several heterocyclic donors such as carbazole derivatives [29–32], phenothiazine [33–36], phenoxazine [37, 38], benzo[1,2-*b*:4,5-*b*']-dithiophene [39] have been exploited for organic dye assembly owing to their exceptional electron-donating ability augmented by little reorganization energy. Recently, dithienopyrrole [40] (DTP) has been suggested as a linker due to its electronic richness and the presence of pyrrolic nitrogen which provides an alternative way for precisely tuning the photophysical properties [41]. To date, DTP have been widely employed as a π-spacer in D–π–A configured dyes [42–48]. However, organic dyes utilizing DTP as an independent donor are limited. Lin and coworkers utilized DTP donor in dianchoring A–D–A motif and reported decent efficiency (3.7%) [49]. Recently, Liang and coworkers used DTP as a terminal donor in two different fashions via *C*-thiophene or *N*-pyrrolic linkage in a D–D–π–A configuration and analyzed the differences in optical and photovoltaic properties. C-linkage proved to be beneficial for extending the absorption edge and molar extinction coefficients than *N*-linkage [50]. However, the *N*-linked dye yielded a high efficiency of 9.02% when cobalt–phenanthroline complex system was used as electrolyte. In this paper, we explore the hitherto unknown D–A_1–π–A dyes where DTP is used as an independent donor via *C*-linkage. Auxiliary acceptors such as BTZ and Qx were used along with thiophene or phenyl unit to compose the conjugation bridge. The use of axillary acceptors in combination with thienyl linker proved to be beneficial for broadening the absorption spectra. A dye containing BTZ and thiophene in the conjugation led to highest efficiency in the series owing to the favorable thermodynamic driving force for electron injection and structural elements helpful to retard electron recombination.

2 Experimental

2.1 Materials and methods

All the chemicals and reagents were received from commercial sources and used without further purification. Organic solvents were purified by following the standard distillation techniques prior to use. Column chromatography purification of synthesized compounds was carried out by using silica gel (100–200 mesh) or neutral alumina as stationary phase in a column of 40 cm length and 3.0 cm diameter. NEXUS FT-IR spectrometer (Thermonicolet) was used to collect IR spectra for the compounds as KBr pellets. The ^{1}H and ^{13}C NMR spectra were recorded on JEOL 400 MHz spectrometer and deuterated chloroform ($CDCl_3$) and dimethyl sulfoxide (DMSO-d_6) were used as solvents. The mass spectra were obtained in a positive ion mode on a Bruker micrOTOF-QII ESI mass spectrometer. UV–visible absorption spectra were obtained by using a Cary 100 spectrophotometer using spectroscopic grade solvents at room temperature in quartz cuvettes. Emission spectra were obtained by using Shimadzu RF5301 spectrofluorimeter. Cyclic voltammetry (CV) and differential pulse voltammetry (DPV) studies were conducted by using BASi Epsilon electrochemical analyzer with a conventional three-electrode configuration consisting of a glassy carbon working electrode, a platinum wire auxiliary electrode, and a non-aqueous $Ag/AgNO_3$ reference electrode. The experiments were performed in dichloromethane at room temperature under nitrogen atmosphere with Bu_4NClO_4 (0.1 M) as supporting electrolyte and the potentials are quoted against the ferrocene which was used as an internal standard.

2.1.1 *Synthesis of 4-(2-butyl-7-(4-(9,9-dibutyl-9H-fluoren-2-yl)-4H-dithieno[3,2-b:2',3'-d]pyrrol-2-yl)-2H-benzo[d][1,2,3] triazol-4-yl)benzaldehyde (2)*

A mixture 4-(7-bromo-2-butyl-2*H*-benzo[*d*][1,2,3] triazol-4-yl)benzaldehyde (**S1**) (0.140 g, 0.40 mmol), **1** (0.80 mmol), $Pd(PPh_3)_2Cl_2$ (0.003 g, 0.04 mmol), and dry DMF (3 mL) was heated at 85 °C under nitrogen atmosphere for 24 h. On the completion of reaction, the reaction mixture was poured into water and organic compound extracted with chloroform. The organic layer was washed with brine solution followed by water and dried over anhydrous Na_2SO_4. The combined organic extracts were concentrated and further purified by column chromatography using alumina as stationary phase and hexanes:chloroform mixture (1:1) as eluent. Red solid; yield 0.205 g (70%).

2.1.2 *Synthesis of 5-(2-butyl-7-(4-(9,9-dibutyl-9H-fluoren-2-yl)-4H-dithieno[3,2-b:2',3'-d]pyrrol-2-yl)-2H-benzo[d][1,2,3] triazol-4-yl)thiophene-2-carbaldehyde (3)*

It was obtained from 5-(7-bromo-2-butyl-2*H*-benzo[*d*][1,2,3] triazol-4-yl)thiophene-2-carbaldehyde (**S2**) (0.300 g, 0.82 mmol) and **1** (1.64 mmol) by following a procedure similar to that described above for the synthesis of **2**. Red solid; yield 0.351 g (61%).

2.1.3 *Synthesis of 4-(2,3-bis(4-(tert-butyl)phenyl)-8-(4-(9,9-dibutyl-9H-fluoren-2-yl)-4H-dithieno[3,2-b:2',3'-d]pyrrol-2-yl)quinoxalin-5-yl)benzaldehyde (4)*

It was obtained from 4-(8-bromo-2,3-bis(4-(*tert*-butyl)phenyl)quinoxalin-5-yl)benzaldehyde (**S3**) (0.160 g, 0.28 mmol) and **1** (0.56 mmol) by following a procedure same as

described above for the synthesis of **2**. Orange solid; yield 0.133 g (50%).

2.1.4 Synthesis of 5-(2,3-bis(4-(tert-butyl)phenyl)-8-(4-(9,9-dibutyl-9H-fluoren-2-yl)-4H-dithieno[3,2-b:2',3'-d]pyrrol-2-yl)quinoxalin-5-yl)thiophene-2-carbaldehyde (5)

It was obtained from 5-(8-bromo-2,3-bis(4-(*tert*-butyl)phenyl)quinoxalin-5-yl)thiophene-2-carbaldehyde (**S4**) (0.140 g, 0.24 mmol) and **1** (0.48 mmol) by following a procedure same as described above for the synthesis of **2**. Dark red solid; yield 0.167 g (73%).

2.1.5 Synthesis (E)-3-(4-(2-butyl-7-(4-(9,9-dibutyl-9H-fluoren-2-yl)-4H-dithieno[3,2-b:2',3'-d]pyrrol-2-yl)-2H-benzo[d][1,2,3] triazol-4-yl) phenyl)-2-cyanoacrylic acid (DTP–TP)

A mixture of **2** (0.140 g, 0.20 mmol), cyanoacetic acid (0.024 g, 0.2 mmol), acetic acid (5 mL) and ammonium acetate (10 mg) was heated at 125 °C for 12 h. The resulting solution was poured into ice-cold water. The precipitate was filtered, washed thoroughly with water and dried. The solid was further crystallized from hot chloroform to get pure compound. Red solid; yield 0.096 g (60%).

2.1.6 Synthesis of (E)-3-(5-(2-butyl-7-(4-(9,9-dibutyl-9H-fluoren-2-yl)-4H-dithieno[3,2-b:2',3'-d]pyrrol-2-yl)-2H-benzo[d][1,2,3] triazol-4-yl) thiophen-2-yl)-2-cyanoacrylic acid (DTP–TS)

It was prepared from **3** (0.150 g, 0.20 mmol) by following a procedure similar to that described above for the synthesis of **DTP–TP**. Black solid; yield 0.103 (72%).

*2.1.7 Synthesis of (E)-3-(4-(2,3-bis(4-(tert-butyl)phenyl)-8-(4-(9,9-dibutyl-9H-fluoren-2-yl)-4H-dithieno[3,2-b:2',3'-d]pyrrol-2-yl)quinoxalin-5-yl)phenyl)-2-cyanoacrylic acid **(DTP–QP)***

It was prepared from **4** (0.120 g, 0.13 mmol) by following a procedure similar to that described above for the synthesis of **DTP–TP**. Brown solid; 0.095 (64%).

*2.1.8 Synthesis of (E)-3-(5-(2,3-bis(4-(tert-butyl)phenyl)-8-(4-(9,9-dibutyl-9H-fluoren-2-yl)-4H-dithieno[3,2-b:2',3'-d]pyrrol-2-yl)quinoxalin-5-yl)thiophen-2-yl)-2-cyanoacrylic acid **(DTP–QS)***

It was prepared from **5** (0.140 g, 0.15 mmol) by following a procedure similar to that described above for the synthesis of **DTP–TP**. Black solid; 0.102 (66%).

2.2 Computational methods

All the computational calculations were performed using Gaussian 09 program package. The ground-state geometries of the dyes were optimized without any symmetry constraints by employing a Becke's hybrid correlation functional B3LYP and 6–31 G(D,P) basis set for all atoms. The vertical excitation energies and oscillator strengths for the lowest 10 singlet–singlet transitions for the optimized geometry in the ground state were obtained by TD-DFT calculations using the DGDZVP basis set and BMK hybrid functional.

2.3 Device fabrication and photovoltaic properties measurements

The dye sensitized TiO_2 photoanodes were prepared by following the procedures present in the literature. A transparent and scattering layers of TiO_2 with different sizes (20 nm and 300 nm, respectively) were coated on a pretreated fluorine-doped SnO_2 conducting glass (FTO, 7 Ω sq.$^{-1}$, transmittance ~80%, NSG America, Inc., New Jersey, USA) by doctor blade technique. During the coating process the dried TiO_2 films firstly was heated at 450 °C in an air flow and then sintered at same temperature for 30 min. The scanning electron microscopic images were used to judge the thickness of TiO_2 layers. The TiO_2 photoanodes of the DSSCs were composed of a 12 μm thick transparent layer and a 4 μm thick scattering layer. After sintering at 450 °C and cooled to 80 °C, The dyes were adsorbed on the TiO_2 film by immersing it in a 3×10^{-4} M dye solution for 24 h, at room temperature. A solvent mixture containing acetonitrile (ACN), *tert*-butyl alcohol and dimethyl sulfoxide (DMSO) (volume ratio of 3.5:3.5:3) was used to prepare the dye bath. The absorption spectra of the dye coated on ~4 μm TiO_2 (20) nm were recorded by using a JASCO UV–visible spectrophotometer (V-570) equipped with an integrating sphere. After that, the TiO_2/dye photoanode was placed over a platinum-sputtered ITO coated glass (7 U Ω sq.$^{-1}$, Ritek Corporation, Hsinchu, Taiwan) and then two electrodes were sandwiched with a 25 mm-thick Surlyn® (SX1170-25, Solaronix S.A., Aubonne, Switzerland) at the edges and sealed by heating. A mixture of 1.2 M 1-propyl-2,3-dimethylimidazolium iodide (DMPII), 0.035 M I_2, 0.5 M *tert*-butylpyridine (TBP) and 0.1 M guanidine thiocyanate dissolved in acetonitrile/3-methoxypropionitrile mixture (8:2) were used as electrolyte. The electrolyte was injected in the gap between the two electrodes through hole which was already made on the counter electrode by drilling machine. After injection of electrolyte the hole was sealed with hot melt-glue to obtain the working DSSC.

The active surface area of the DSSC was restricted to 0.16 cm^2 by using a mask. The DSSC was illuminated by a class-A solar simulator (XES-301S, AM 1.5 G, San-Ei Electric Co., Ltd.). A standard silicon cell (PECSI01, Peccell

Technologies, Inc.) was used to calibrate the incident light intensity of simulator and maintained at 100 mW cm^{-2}. A potentiostat/galvanostat (PGSTAT30, Autolab, Eco-Chemie, Netherlands) was used to characterize the Photocurrent-voltage curves of the DSSC. A potentiostat/galvanostat equipped with an FRA2 module was employed to analyze electrochemical impedance spectral (EIS) analysis of the DSSCs. The applied bias voltage was set at the open-circuit voltage between the working photoanode and Pt-counter electrode of the DSSC under a constant light illumination 100 mW cm^{-2}. Incident photocurrent conversion efficiency (IPCE) spectrum was obtained using a monochromated light (Oriel Instrument, model 74100) at short-circuit condition. The IPCE (λ) is defined by IPCE (λ) = 1240 (J_{SC}/λφ), where λ is the wavelength, J_{SC} is short-circuit photocurrent density (mA cm^{-2}) recorded with a potentiostat/galvanostat, and φ is the incident radiative flux (Wm^{-2}) measured with an optical detector (Oriel Instrument, model 71580) and a power meter (Oriel Instrument, model 70310).

3 Results and discussion

3.1 Molecular design and synthesis

The structures of the newly synthesized organic dyes containing dithienopyrrole donor and different π-conjugation bridges and cyanoacrylic acid acceptor are displayed in Fig. 1. The methodology used to obtain the target dyes is outlined in the Scheme 1. All the target dyes were obtained by multi-step sequence involving conventional reactions such as Vilsmeier–Haack formylation, Suzuki–Miyaura [51]/Stille [52] cross-coupling and Knoevenegal [53] condensation. The key precursor 4-(9,9-dibutyl-9*H*-fluoren-2-yl)-2-(tributylstannyl)-4*H*-dithieno[3,2-*b*:2′,3′-*d*]pyrrole (**1**) was synthesized from 4-(9,9-dibutyl-9*H*-fluoren-2-yl)-4*H*-dithieno[3,2-*b*:2′,3′-*d*]pyrrole [47] by a known procedure [54]. The aldehyde precursors **2–5** were synthesized by following Stille coupling protocol involving **1** and different bromo-arene/heteroarene–aldehydes **S1-S4**. Finally, the aldehydes, **2–5** were converted into the target dyes **DTP–TP, DTP–TS, DTP–QP** and **DTP–QS**, on reaction with cyanoacetic acid in the presence of catalytic amount of ammonium acetate. All the newly synthesized dyes were thoroughly characterized by ^{1}H, ^{13}C NMR spectroscopy, FT-IR, and HR mass spectra. The analytical data (Table 1) observed are consistent with the proposed structures of the compounds.

3.2 Optical properties

To investigate the light harvesting efficiency of the synthesized dyes, the absorption spectra of the dyes were recorded in dichloromethane (DCM) and displayed in Fig. 2. The

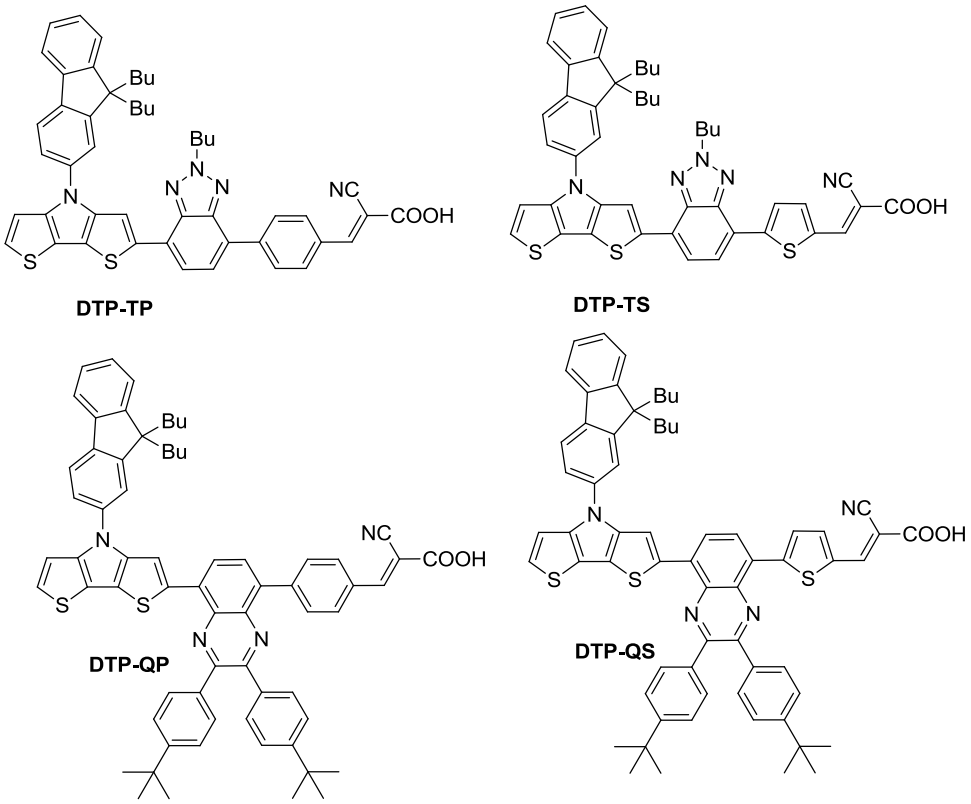

Fig. 1 Structures of dyes featuring DTP donor in a D–A–π–A configuration

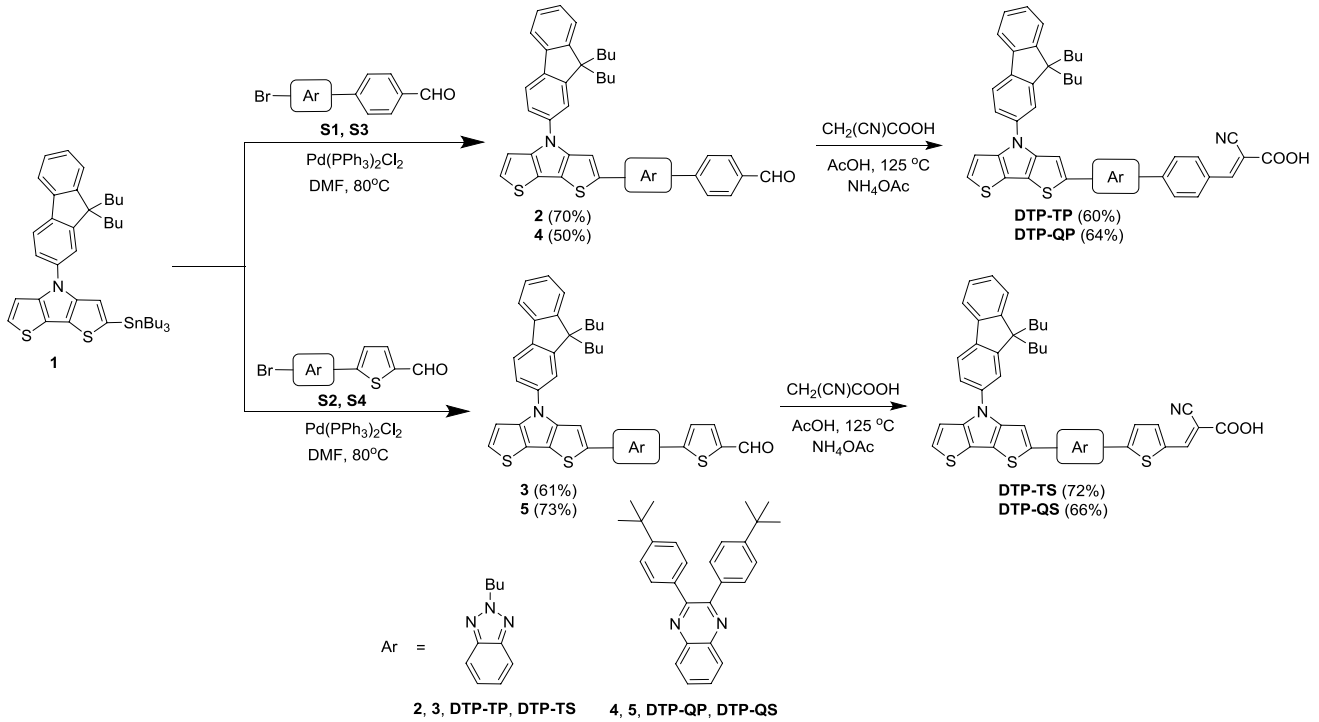

Scheme 1 Synthetic scheme of the dyes

pertinent optical data were compiled in Table 2. Generally, the absorption of the dyes spread over region, 285–620 nm. At least two prominent absorptions were observed. The absorption peak appearing at shorter wavelength region (<400 nm) can be assigned to π–π* electronic transition arising from different aromatic segments present in the dyes while the absorption in the longer wavelength region (above 403 nm) is ascribed to the intramolecular charge transfer (CT) from DTP donor to the cyanoacrylic acid acceptor [13]. The dyes **DTP–TS** and **DTP–QS** containing thienyl π-linker exhibited intense and broader absorption profile as compared to phenyl-linked dyes (**DTP–TP** and **DTP–QP**) [55]. This is because of the presence of electron-rich thienyl π-linker which facilitates electronic communication between DTP donor and cyanoacrylic acceptor due to its planar arrangement. On the other hand in the phenyl-linked dyes (**DTP–TP** and **DTP–QP**), the twisted arrangement of phenyl unit reduces the donor–acceptor interactions and shift the ICT absorption band to the shorter wavelength region. The BTZ dyes (**DTP–TS** and **DTP–TP**) displayed relatively high molar extinction coefficients for the ICT band when compared to the similar Qx-dyes (**DTP–QS** and **DTP–QP**). It is probable that the Qx unit is not suitable to render an effective pathway for electronic communication between the donor and acceptor.

The charge-transfer character of the longer wavelength absorption was confirmed by comparing the absorption spectra of their respective aldehyde precursors. Pronounced bathochromic shifts for the absorption were noticed on converting the aldehyde to stronger electron-withdrawing cyanoacrylic acid group. This cannot arise only due to the extension in conjugation. Further, the acid-base equilibrium analyses carried out by recording the absorption spectra of the dyes in the presence of TFA/TEA (Fig. 3). All the dyes displayed pronounced blue-shift on addition of TEA and a slight red-shift with TFA for the CT absorption. These are attributed to decrement/increment in the acceptor strength originating from the deprotonation/protonation on addition of TEA/TFA. Also, the dyes exhibited negative solvatochromism (Fig. 4) in the ground state attributable to the effective solvation of the dyes in ground state by more polar solvents [56]. However, the dyes showed distinctively blue-shifted absorption in MeOH and DMF arising from the hydrogen-bonding and basic nature of the solvent, respectively. Additionally, the most red-shifted absorption was observed in chlorinated solvent (DCM) owing to the fast reorganization of polarized electrons in the excited state of the dyes [57].

The absorption spectra of the dyes recorded on mesoporous thin film of nanocrystalline TiO_2 are displayed in Fig. 5. The absorption maxima for the dye on TiO_2 were red-shifted and broadened when compared to the absorption in solution. This can be attributed to the *J*-aggregation of the dyes on TiO_2 surfaces [58]. All the dyes are weakly emissive in the solution and the trend in emission peak is similar to that observed for absorption. Since the dyes feature ICT

Table 1 Analytical data of the intermediates and dyes

Compound	Melting point (°C)	IR (KBr, cm^{-1})	δ_H ($CDCl_3$, ppm)	δ_C ($CDCl_3$, ppm)	m/z	
					Calculated	Found
2	105–107	1697 ($\nu_{C=O}$)	0.70–0.76 (m, 10 H), 1.00-1.04 (m, 3 H), 1.09–1.16 (m, 4 H), 1.26–1.32 (m, 2 H), 2.04–2.09 (m, 4 H), 2.19 (t, $J=7.2$ Hz, 2 H), 4.82–4.85 (m, 2 H), 7.20 (d, $J=5.6$ Hz, 1 H), 7.28 (d, $J=5.6$ Hz, 1 H), 7.36–7.42 (m, 3 H), 7.65–7.69 (m, 3 H), 7.75–7.78 (m, 2 H), 7.89 (d, $J=8.0$ Hz, 1 H), 8.04 (d, $J=8.4$ Hz, 2 H), 8.27 (d, $J=8.4$ Hz, 2 H), 8.32 (s, 1 H), 10.08 (s, 1 H)	192.1, 152.7, 150.8, 144.7, 143.4, 140.4, 139.3, 138.8, 135.4, 130.2, 129.2, 129.0, 127.7, 127.1, 126.5, 125.6, 124.7, 123.1, 121.9, 121.6, 120.8, 119.8, 117.4, 112.9, 112.4, 56.7, 55.4, 40.3, 32.5, 32.2, 32.0, 29.8, 29.7, 26.2, 23.2, 23.07, 23.0, 22.8, 20.0, 14.2	755.2848 ($C_{46}H_{44}N_4OS_2$ $[M+Na]^+$)	755.2841
3	135–137	1660 ($\nu_{C=O}$)	0.68–0.77 (m, 10 H), 1.00-1.04 (m, 3 H), 1.09–1.16 (m, 4 H), 1.46–1.55 (m, 2 H), 2.04–2.08 (m, 4 H), 2.16–2.23 (m, 2 H), 4.84 (t, $J=7.2$ Hz, 2 H), 7.19 (d, $J=5.2$ Hz, 1 H), 7.27 (d, $J=5.2$ Hz, 1 H), 7.34–7.41 (m, 3 H), 7.64–7.69 (m, 3 H), 7.75–7.78 (m, 2 H), 7.82 (d, $J=4.4$ Hz, 1 H), 7.88 (d, $J=8.0$ Hz, 1 H), 8.15 (d, $J=4.0$ Hz, 1 H), 8.31 (s, 1 H), 9.94 (s, 1 H)	183.0, 152.6, 150.7, 149.7, 144.8, 144.8, 144.6, 142.3, 142.1, 141.7, 140.2, 139.3, 138.6, 137.3, 137.1, 127.3, 127.1, 127.1, 127.0, 124.9, 124.4, 123.0, 121.5, 121.3, 120.7, 119.7, 118.0, 117.1, 113.0, 112.24, 56.7, 55.3, 40.2, 32.0, 26.1, 23.1, 19.9, 13.9, 13.6	738.2515 ($C_{44}H_{42}N_4OS_3$ $[M]^+$)	738.2520
4	170–172	1644 ($\nu_{C=O}$)	0.71–0.74 (m, 10 H), 1.10–1.19 (m, 4 H), 1.25 (s, 9 H), 1.31 (s, 9 H), 2.04 (t, $J=8.0$ Hz, 4 H), 7.20 (d, $J=5.2$ Hz, 1 H), 7.28–7.33 (m, 2 H), 7.35–7.41 (m, 5 H), 7.54 (d, $J=8.0$ Hz, 2 H), 7.64 (s, 1 H), 7.70–7.78 (m, 4 H), 7.82 (d, $J=8.0$ Hz, 1 H), 7.91 (d, $J=8.0$ Hz, 1 H), 8.04 (s, 5 H), 8.16 (d, $J=7.6$ Hz, 1 H), 8.26 (s, 1 H), 10.12 (s, 1 H)	192.5, 152.5, 150.9, 144.1, 138.8, 138.7, 137.3, 137.2, 136.0, 135.8, 135.2, 133.8, 131.6, 130.6, 130.1, 130.0, 129.7, 129.5, 129.2, 127.4, 127.3, 127.1, 126.4, 126.1, 125.9, 125.4, 125.3, 124.5, 123.1, 121.6, 120.8, 119.9, 117.7, 112.6, 55.4, 40.3, 31.3, 29.8, 26.2, 23.2, 14.1, 14.0	974.4148 ($C_{64}H_{61}N_3OS_2$ $[M+Na]^+$)	974.4140
5	100–102	1664 ($\nu_{C=O}$)	0.71–0.77 (m, 10 H), 1.12–1.17 (m, 4 H), 1.32 (s, 9 H), 1.36 (s, 9 H), 2.02–2.06 (m, 4 H), 7.19 (d, $J=5.2$ Hz, 1 H), 7.29 (d, $J=6.0$ Hz, 1 H), 7.37–7.43 (m, 8 H), 7.63 (d, $J=2.0$ Hz, 1 H), 7.67–7.73 (m, 4 H), 7.78 (d, $J=6.8$ Hz, 1 H), 7.81 (d, $J=4.0$ Hz, 1 H), 7.91 (t, $J=4.0$ Hz, 2 H), 8.11 (s, 2 H), 8.25 (s, 1 H), 9.98 (s, 1 H)	183.5, 152.8, 152.7, 152.6, 150.9, 148.8, 144.9, 144.8, 144.5, 140.3, 139.4, 137.3, 137.1, 135.9, 135.6, 135.6, 134.1, 130.2, 128.9, 128.0, 127.4, 127.9, 127.1, 126.9, 125.8, 125.6, 125.5, 125.4, 125.2, 125.1, 124.8, 123.0, 121.7, 121.0, 120.9, 119.9, 117.7, 117.3, 112.8, 112.2, 55.4, 40.3, 34.9, 31.4, 29.8, 26.2, 23.2, 14.2	980.3712 ($C_{62}H_{59}N_3OS_3$ $[M+Na]^+$)	980.3706

Table 1 (continued)

Compound	Melting point (°C)	IR (KBr, cm^{-1})	δ_H ($CDCl_3$, ppm)	δ_C ($CDCl_3$, ppm)	m/z	
					Calculated	Found
DTP–TP	215–217	2219 ($\nu_{C\equiv N}$)	0.53–0.64 (m, 10 H), 0.86–0.92 (m, 3 H), 1.00-1.09 (m, 4 H), 1.31–1.40 (m, 2 H), 2.02–2.17 (m, 6 H), 4.84 (t, $J=7.2$ Hz, 2 H), 7.25 (d, $J=5.6$ Hz, 1 H), 7.33–7.39 (m, 2 H), 7.47–7.49 (m, 1 H), 7.58 (d, $J=5.2$ Hz, 1 H), 7.70 (d, $J=8.4$ Hz, 1 H), 7.82–7.89 (m, 4 H), 8.03 (d, $J=8.0$ Hz, 1 H), 8.14 (d, $J=8.4$ Hz, 2 H), 8.29–8.34 (m, 4 H)	163.8, 152.8, 150.8, 144.9, 144.2, 142.9, 141.8, 140.9, 140.3, 139.4, 138.4, 137.1, 131.5, 131.5, 129.0, 127.7, 127.1, 127.0, 125.9, 123.5, 122.4, 121.8, 120.5, 117.9, 117.5, 117.0, 113.0, 112.9, 55.7, 55.4, 32.1, 26.4, 23.0, 22.6, 19.8, 14.3, 13.9	800.3087 ($C_{49}H_{45}N_5O_2S_2$ $[M+H]^+$)	822.3111
DTP–TS	250–252	2217 ($\nu_{C\equiv N}$)	0.38–0.63 (m, 10 H), 0.89–0.93 (m, 4 H), 1.00-1.07 (m, 3 H), 1.29–1.41 (m, 2 H), 2.02–2.14 (m, 6 H), 4.81–4.83 (d, $J=6.4$ Hz, 2 H), 7.22–7.38 (m, 4 H), 7.48 (d, $J=6.0$ Hz, 1 H), 7.54–7.57 (m, 1 H), 7.67–7.88 (m, 4 H), 7.98–8.04 (m, 2 H), 8.15 (t, $J=4.0$ Hz, 1 H), 8.23–8.26 (m, 1 H), 8.40 (s, 1 H)	164.1, 152.8, 155.5, 150.8, 145.7, 145.0, 144.2, 141.7, 141.3, 140.3, 139.3, 138.3, 136.9, 136.3, 127.9, 127.6, 127.2, 126.3, 125.0, 124.0, 123.5, 122.1, 122.0, 121.8, 121.7, 121.0, 120.5, 118.2, 117.6, 117.4, 117.0, 113.2, 112.9, 56.7, 55.3, 31.7, 26.4, 23.0, 19.9, 14.3, 13.9	828.2471 ($C_{47}H_{43}N_5O_2S_3$ $[M+Na]^+$)	828.2491
DTP–QP	218–220	2219 ($\nu_{C\equiv N}$)	0.54–0.65 (m, 10 H), 0.99–1.08 (m, 4 H), 1.15 (s, 9 H), 1.22 (s, 9 H), 1.95–2.01 (m, 2 H), 2.07–2.14 (m, 2 H), 7.22–7.30 (m, 5 H), 7.33–7.39 (m, 4 H), 7.46–7.48 (m, 1 H), 7.52 (d, $J=8.4$ Hz, 2 H), 7.59 (d, $J=5.2$ Hz, 1 H), 7.66 (d, $J=7.6$ Hz, 1 H), 7.75 (s, 1 H), 7.80 (d, $J=7.6$ Hz, 1 H), 7.88 (d, $J=6.4$ Hz, 1 H), 7.94–7.98 (m, 2 H), 8.02 (d, $J=8.0$ Hz, 1 H), 8.11–8.15 (m, 3 H), 8. 33 (s, 1 H), 8.37 (s, 1 H)	163.9, 154.1, 152.8, 152.3, 152.1, 151.4, 151.0, 144.8, 144.1, 142.7, 140.3, 139.3, 138.8, 132.8, 131.8, 131.1, 130.7, 130.2, 129.8, 127.9, 127.6, 126.7, 125.5, 125.4, 123.5, 121.9, 121.7, 120.6, 119.7, 117.7, 117.0, 116.9, 113.8, 112.81, 112.77, 55.5, 34.9, 31.6, 26.4, 23.0, 14.3	1041.4206 ($C_{67}H_{62}N_4O_2S_2$ $[M+Na]^+$)	1041.4214
DTP–QS	232–235	2224 ($\nu_{C\equiv N}$)	0.72–0.74 (m, 10 H), 1.12–1.16 (m, 4 H), 1.37 (d, $J=1.6$ Hz, 18 H), 2.07–2.15 (m, 4 H), 7.42–7.49 (m, 4 H), 7.57–7.72 (m, 11 H), 7.76–7.82 (m, 1 H), 7.89–8.01 (m, 4 H), 8.35–8.50 (m, 2 H), 8.66 (s, 1 H)	153.0, 150.6, 150.3, 150.2, 146.4, 130.1, 129.9, 129.8, 129.6, 129.52, 129.46, 129.3, 127.5, 127.4, 127.1, 127.0, 126.5, 126.4, 122.9, 122.4, 121.6, 120.6, 119.7, 117.6, 114.8, 112.2, 55.2, 39.9, 22.7, 13.43, 13.37	1047.3776 ($C_{65}H_{60}N_4O_2S_3$ $[M+Na]^+$)	1047.3796

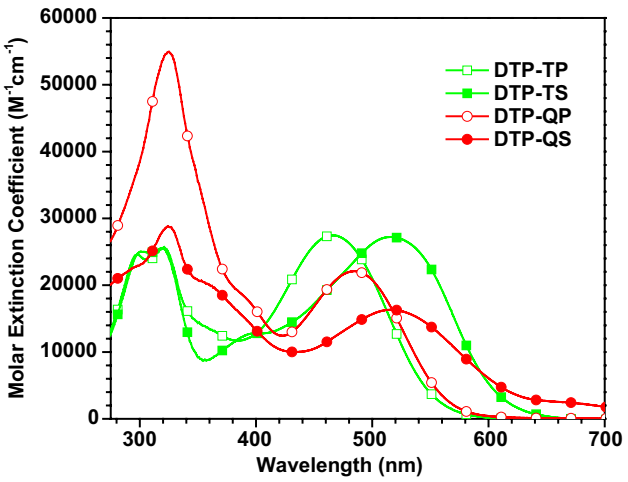

Fig. 2 Absorption spectra of the dyes recorded in dichloromethane

excited state which is prone of dipole–dipole relaxation with the solvent dipoles [59].

3.3 Electrochemical properties

The molecular orbital energies give insightful information about the propensity of electron injection from the excited dyes into the conduction band (CB) of TiO_2 and regeneration of oxidized dyes by electrolyte. These parameters can be calculated from the oxidation and reduction potentials which corresponds to highest occupied molecular orbital (HOMO) and lowest unoccupied molecular orbital (LUMO), respectively. Therefore, we carried out the cyclic voltammetry (CV) and differential pulse voltammetry (DPV) measurements on the dyes in DCM solutions. The relevant parameters and the derived orbital energies are presented in Table 2. BTZ-based dyes showed a quasi-reversible oxidation while the Qx-containing dyes exhibited an irreversible oxidation attributable to the removal of an electron from dithienopyrrole donor (Fig. 6). Irreversibility of the oxidation in Qx-based dyes indicates that they undergo severe reorganization upon oxidation. However, the oxidation potentials do not show variations attributable to the nature of electron-withdrawing linker. It apparently points that the electron-accepting ability of BTZ and Qx units are almost same [60]. But the additional linker such as phenyl and thiophene units marked their presence in the oxidation potentials of the dyes. A slightly lower oxidation potentials observed for the dyes containing phenyl linker is attributed to the poor electronic communication between the donor and acceptor because of the tilting in the phenyl ring. Lack of strong interaction between the donor and acceptor makes the donor comparatively electron-rich and so oxidized easily.

The excited state oxidation potentials (E^*_{OX}) obtained by the equation $E^*_{OX} = E_{OX} - E_{0-0}$, where E_{0-0} was calculated from intersection of normalized absorption and emission spectra of the dyes. It is interesting to note that the thienyl-linked dyes (**DTP–TS** and **DTP–QS**) exhibited lower E^*_{OX} values than the corresponding phenyl analogues due to the better donor–acceptor interactions induced by the planner thienyl linker. The lowering of the E^*_{OX} values resulted in decrease in the energy band gap for these dyes which is consistent with absorption of these dyes. The ground state oxidation potentials for the dyes are sufficiently more positive (~1.20 V vs. NHE) than the redox potential of I^-/I_3^- electrolyte (0.4 V vs. NHE) [61] which attests the thermodynamic

Table 2 Optical and electrochemical data of the dyes

Dyes	λ_{abs} [nm, ε_{max} ($\times 10^3$ M^{-1} cm^{-1})]	$\lambda_{max}^{TiO_2}$ (nm)	E_{OX}[a] [mV, ΔE_p[b] (mV)]	HOMO[c] (eV)	LUMO[d] (eV)	E_{0-0}[e] (eV)	E_{OX}[f] [V, (Vs NHE)]	E^*_{OX}[g] [V, (Vs NHE)]	ΔG_{inj}[h] (V)
DTP–TP	298 (24.6), 321 (25.7), 465 (27.5)	520	425 (136)	5.225	2.720	2.505	1.195	−1.231	0.731
DTP–TS	301 (25.0), 318 (25.5), 403 (12.8), 516 (27.2)	545	434 (135)	5.234	2.975	2.259	1.204	−1.055	0.555
DTP–QP	325 (54.9), 485 (22.1)	515	428 (086)	5.228	2.816	2.412	1.198	−1.214	0.714
DTP–QS	324 (28.8), 516 (16.3)	535	431 (083)	5.231	3.122	2.109	1.201	−0.908	0.408

[a]Oxidation potentials are reported with reference to the ferrocene internal standard

[b]Peak-to-peak separation

[c]Deduced from the oxidation potential using the formula $HOMO = 4.8 + E_{OX}$

[d]Deduced using the formula $LUMO = HOMO - E_{0-0}$

[e]Calculated from intersection of absorption and emission spectra

[f]Calculated by the addition of solvent correction (0.77 for DCM) to E_{OX}

[g]Calculated from $E^*_{OX} = E_{OX} - E_{0-0}$

[h]Free energy change for the electron injection process, $\Delta G_{inj} = E_{CB} - E^*_{OX}$ where E_{CB} is the conduction band edge of TiO_2 and we used the value of –0.5 V.

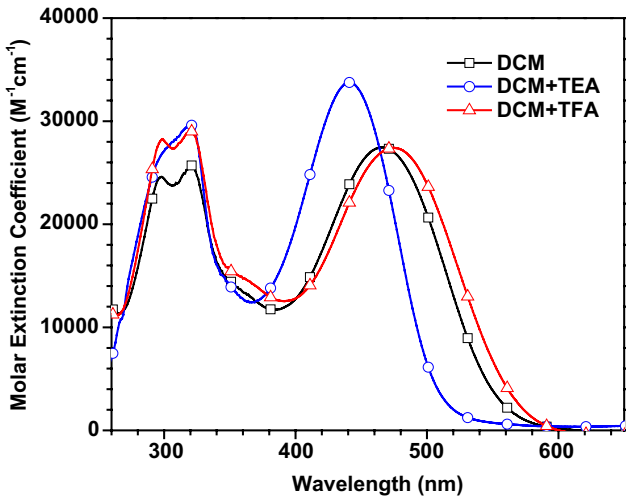

Fig. 3 Absorption spectra of the dye **DTP–TP** recorded in DCM before and after the addition of TEA/TFA

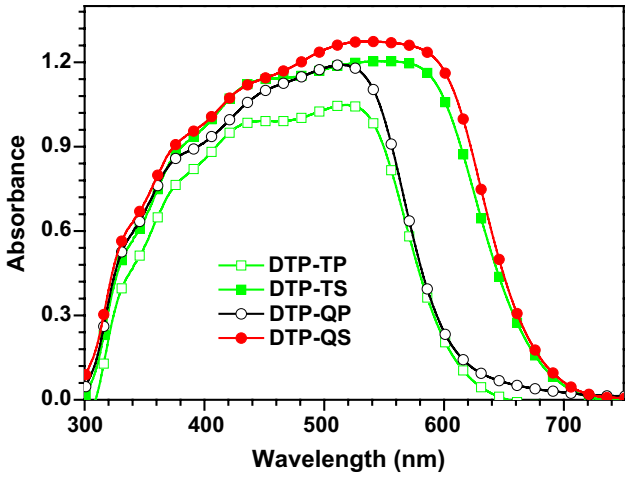

Fig. 5 Absorption spectra of the dyes anchored on nanocrystalline TiO_2

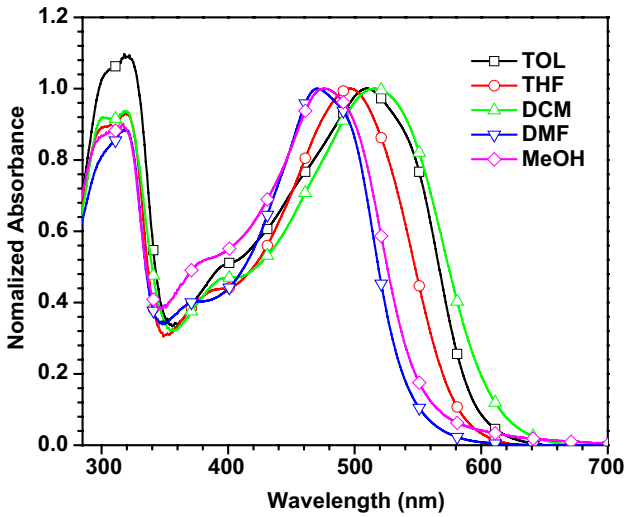

Fig. 4 Normalized absorption spectra of the dye **DTP–TS** dye recorded in different solvents

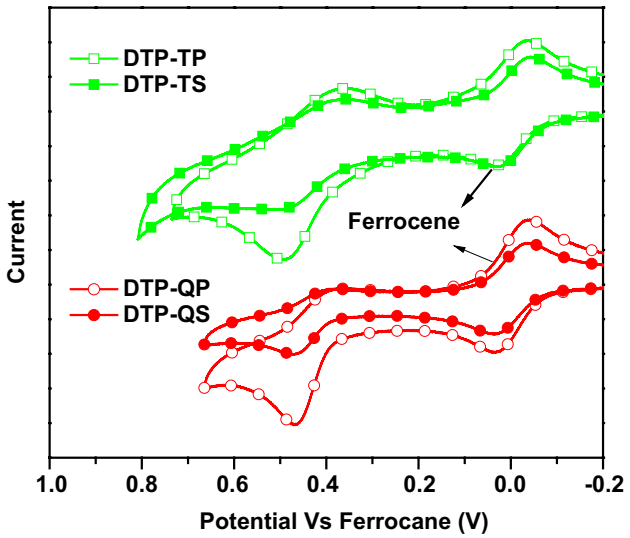

Fig. 6 Cyclic voltammograms of the dyes recorded in dichloromethane

feasibility for the regeneration of the oxidized dye by the electrolyte (Fig. 7). The excited state oxidation potentials of the sensitizers are more negative (−0.91 to −1.23 V vs. NHE) than the conduction band edge (−0.5 V vs. NHE) [62] of TiO_2, which energetically permits the injection of electron from the excited state of the sensitizers into the conduction band of the TiO_2.

3.4 Theoretical calculations

To elucidate the nature of oxidation and absorption in the dyes, the electronic structure calculations were performed at the density functional theory [63, 64] level using B3LYP/6–31 g(d,p) hybrid functional. The HOMO and LUMO electronic distributions for the dyes containing different π-conjugation are depicted in Fig. 8. The HOMO of the dyes are mainly contributed by the DTP unit and spread over the benzene ring of the BTZ or Qx segments. The LUMO of the dyes are mainly concentrated on cyanoacrylic acid and spread up to the auxiliary acceptor via the phenyl or thiophene linker. The significant overlap of HOMO and LUMO over the auxiliary acceptor ensure the migration of charge from the DTP donor to the cyanoacrylic acid acceptor via the linker. However, the twisting of phenyl π-linkers in the dyes (**DTP–TP**, and **DTP–QP**) may reduce the transition probability of CT. The blue shifted absorption observed

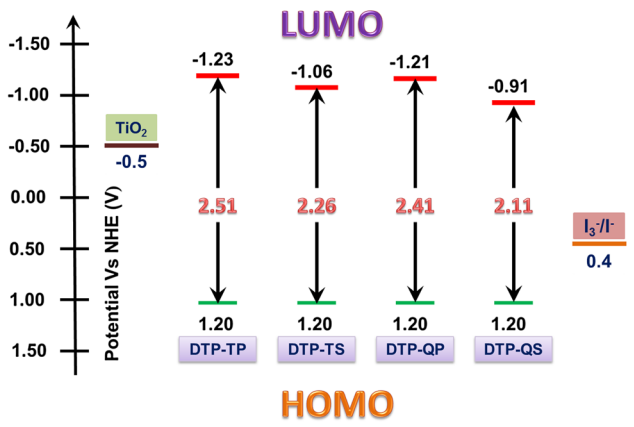

Fig. 7 Energy level diagram for the dyes

for the phenyl-linked dyes (**DTP–TP**, and **DTP–QP**) attests this hypothesis.

To predict the absorption wavelengths and estimate the trend among the compounds the electronic excitation parameters were computed using the time-dependent density functional theory (TD-DFT) employing BMK functional and DGDZVP basis set. The computed excitation energies, their oscillator strength (*f*) and molecular orbital contributions are listed in Table 3. The calculated maximum wavelength absorption follows the trend **DTP–QS > DTP–TS > DTP–TP > DTP–QP** which is similar to the observed values in THF. Also, the charge transfer nature of the longer wavelength absorption is confirmed from the orbital contributions to this transition.

3.5 Photovoltaic properties

To investigate the photovoltaic properties of the dyes, we fabricated the DSSCs by employing the dyes as sensitizers and the performance parameters summarized in Table 4. The incident photon-to-current conversion efficiencies (IPCE) of the DSSCs as function of different irradiation wavelengths is plotted in Fig. 9. The IPCE spectrum of a particular dye depends on the light harvesting efficacy of the dye, thus the obtained superior spectral response of BTZ-based dyes is attributed to the comparatively high molar extinction coefficients observed when compared to the Qx-based dyes. Also, the thiophene-linked dyes (**DTP–TS** and **DTP–QS**) exhibited longer wavelength onset for IPCE which is in accordance with low energy tailing of their absorption. The

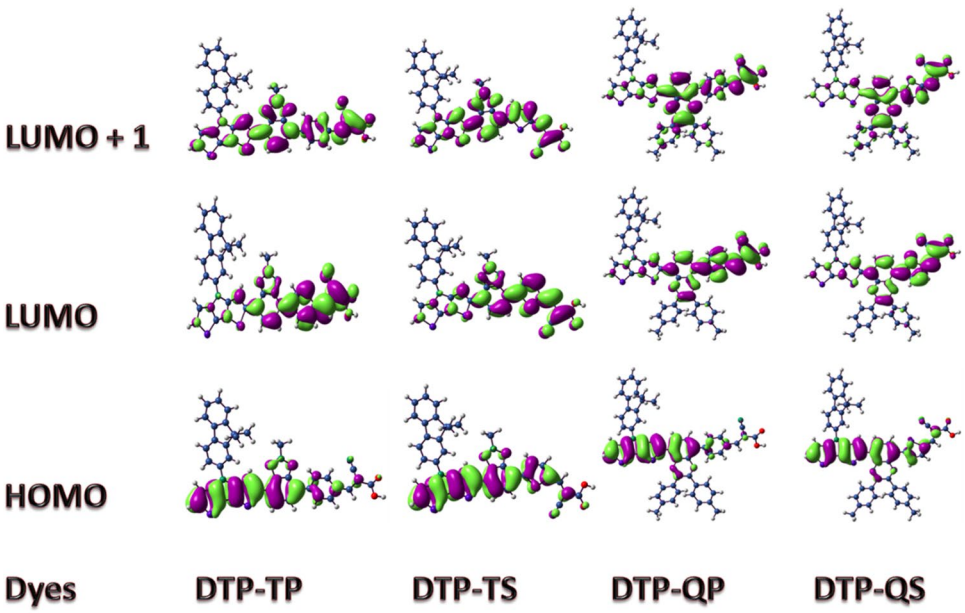

Fig. 8 Electronic distribution in the frontier molecular orbitals of the dyes

Table 3 Computed vertical transition energies and their oscillator strengths and configurations for the dyes

Dye	λ_{max}^{abs} (nm)	*f*	Configuration	HOMO (eV)	LUMO (eV)	Band gap (eV)
DTP–TP	482	1.73	HOMO→LUMO (89%)	−5.93	−2.37	3.57
DTP–TS	536	1.74	HOMO→LUMO (93%)	−5.93	−2.59	3.34
DTP–QP	481	1.18	HOMO→LUMO (83%), HOMO→LUMO + 1 (13%)	−5.91	−2.32	3.59
DTP–QS	539	1.29	HOMO→LUMO (92%)	−5.93	−2.37	3.57

Table 4 Performance parameters of the DSSCs fabricated with synthesized dye

Dye	J_{SC} (mA cm^{-2})	V_{OC} (mV)	*FF*	η (%)	R_{ct2} (Ω)	τ_e (ms)	R_{rec} (Ω)
DTP–TP	6.07	598.6	0.64	2.33	29.63	3.34	37.76
DTP–TS	7.13	618.1	0.59	2.61	28.25	4.39	45.79
DTP–QP	4.62	605.9	0.65	1.83	42.11	3.34	39.75
DTP–QS	4.98	598.6	0.66	1.97	39.52	3.34	37.76

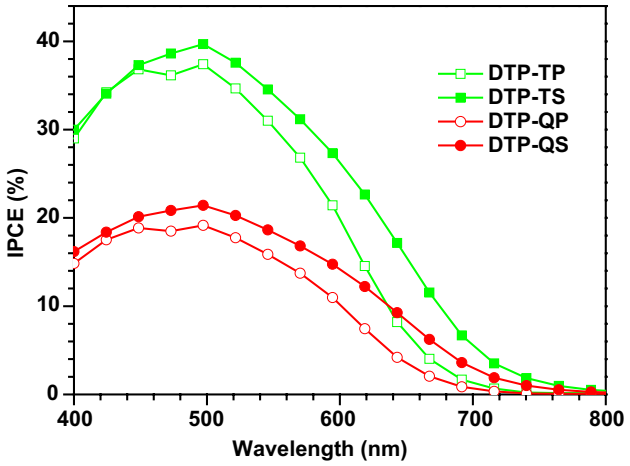

Fig. 9 IPCE spectra of the DSSCs fabricated with the dyes

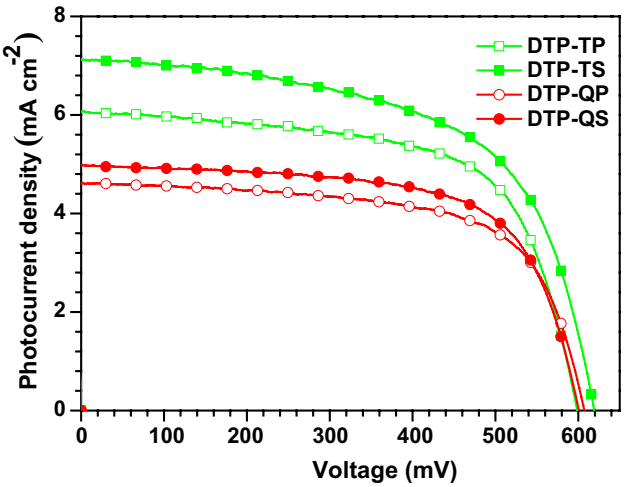

Fig. 10 I–V characteristics of the DSSCs fabricated with the dyes

current–voltage (I–V) characteristics were measured under simulated solar light conditions and presented in Fig. 10. The photocurrent density of the dyes assume the order, **DTP–TS > DTP–TP > DTP–QS > DTP–QP**. The better J_{SC} observed for the dyes **DTP–TP** and **DTP–TS** is attributed to their broad and intense absorption. On the other hand, inferior molar extinction coefficients and poor electronic coupling with the TiO_2 nanoparticles may be responsible for low photocurrent density observed of the dyes, **DTP–QS** and **DTP–QP** [65]. The presence *n*-butyl group BTZ unit and bulky *tert*-butylphenyl group on Qx respectively are expected to retard the approach of electrolyte and dye aggregation on the TiO_2 surface and improve the open circuit voltage. The trend for the open circuit voltage of the dyes is, **DTP–TS > DTP–QP > DTP–TP = DTP–QS**. It is interesting to note that the **DTP–TS** exhibited the highest V_{OC} among the series. Since all the dyes possesses similar HOMO energy levels, the dye regeneration cannot be a deciding factor for the observed trend of V_{OC} but can be explained on the basis of electron life time and charge collection efficiency (*vide infra*).

3.6 Electrochemical impedance spectroscopy

To further understand the structural effect of different π-linkers on the fate of electrons at the interfaces of the DSSCs, we carried out the electrochemical impedance spectroscopy (EIS) measurements under dark and one sun illumination conditions. The Nyquist plots obtained in dark and illumination conditions are displayed in Figs. 11 and 12, respectively. The electron recombination resistances (R_{rec}) at the interfaces of TiO_2/dye/electrolyte correspond to the second semicircle in Fig. 11. The diameter of this semicircle is the measure of recombination resistance. The order of R_{rec} is **DTP–TS > DTP–QP > DTP–TS = DTP–QS**, which is consistent with the V_{OC} trend. The largest R_{rec} value obtained for the dye **DTP–TS** suggests that BTZ unit in conjunction with thienyl linker effectively suppresses the recombination of electrons with the oxidized electrolyte. Also, the superior harvesting ability of **DTP–TS** may also increase the electron density in the TiO_2 conduction band and upwardly shift the fermi energy. If this is true this dye should display better charge collection efficiency and longer electron life time [66, 67]. Charge-transport resistance (R_{ct2}) for the DSSCs are estimated from the large semicircle of the Nyquist plots constructed from the data collected under the one sun illumination conditions (Fig. 12). The R_{ct2} of the dyes followed the order, **DTP–QP > DTP–QS > DTP–TP > DTP–TS**. The comparatively smaller R_{ct2} values for the BTZ dyes suggest efficient charge collection in those devices. On comparing the linkers, the phenyl containing dyes (**DTP–QP** and **DTP–TP**) possessed larger R_{ct2} values when compared to their thiophene counter parts (**DTP–QS**

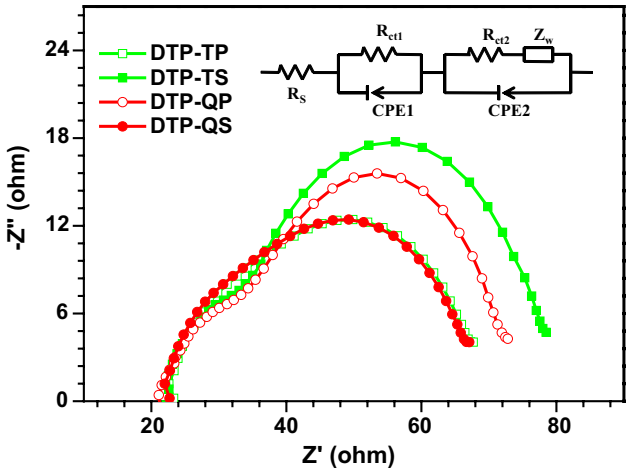

Fig. 11 Nyquist plots observed for the DSSCs under dark condition

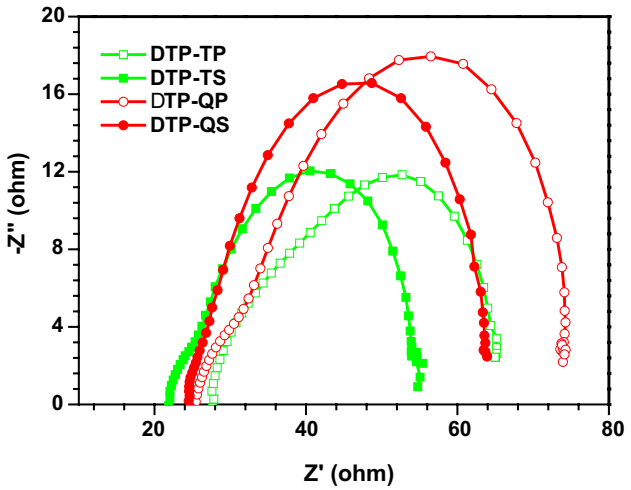

Fig. 12 Nyquist plots observed for the DSSCs under illumination

and **DTP–TS**). This originates from the unfavorable thermodynamic condition due to the relatively high-lying LUMO of them [68, 69]. The electron life time (τ_e) in the device can be measured by the mid-frequency peaks of the Bode phase plot (Fig. 13) from the equation $\tau_e = 1/\omega_{min}$, where ω_{min} is the angular frequency of low frequency peak [70, 71]. The dye **DTP–TS** showed highest τ_e value suggestive of more effective suppression of the back electron transfer when compared to the other dyes. Thus the BTZ-thiophene dyad is constituting to an efficient conjugation pathway leading to improved electronic coupling between the donor and acceptor and inhibition of recombination of electrons. Thus, the efficient performance of **DTP–TS** in DSSC may be ascribed to the effective injection of electrons into the conduction band of TiO_2 and aggressive reduction of recombination of electrons with the electrolyte.

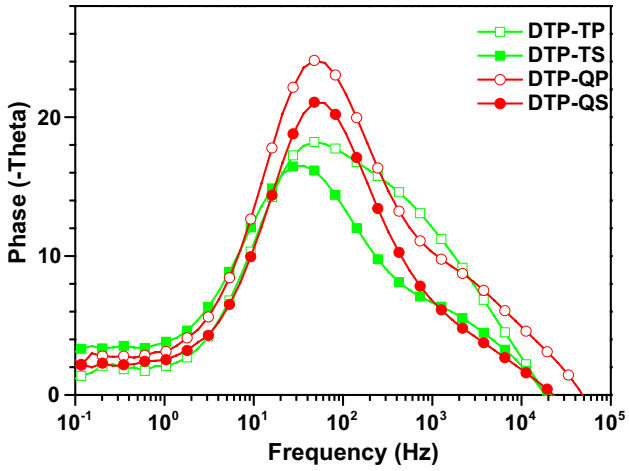

Fig. 13 Bode phase plots for the DSSCs measured under illumination

4 Conclusions

In summary, we demonstrated the use of fluorene-substituted dithienopyrrole as a donor in organic dyes featuring D–A–π–A structural organization employing different electron-demanding linkers such as BTZ and Qx along with cyanoacrylic acid acceptor. The incorporation of an auxiliary acceptor along with electronic rich thienyl unit is found to facilitate donor–acceptor interactions and modulate the absorption characteristics. Theoretically, it was established that more delocalization of HOMO in the BTZ-based dyes were beneficial for charge transfer to acceptor due to enhanced overlap with LUMO. The dyes were found to be sufficiently polar in the ground state as confirmed by the negative solvatochromism exhibited by them in the absorption spectra. The LUMO energies of the dyes showed significant variations attributable to the nature of linker. Consequently, the dyes possessing BTZ and thiophene linkers exhibited relatively low-lying LUMO and increased the charge injection propensity due to the favorable thermodynamic driving force. Among the dyes, **DTP–TS** displayed high photocurrent density and open circuit voltage and hence highest power conversion efficiency. The superior performance of **DTP–TS** is attributed to the large recombination resistance and low charge transfer resistance by EIS studies. This work suggests that by the choice of linkers the photovoltaic properties of the organic dyes can be effectively tuned.

Acknowledgements K.R.J.T. is thankful to CSIR (Ref. 02/(0230)/15/EMR-II dated 05-06-2015), New Delhi and Department of Science and Technology (Ref. DST/TSG/PT/2013/09), New Delhi, India for financial support. S.K. acknowledges a Senior Research Fellowship from UGC, New Delhi. Financial support from DST, New Delhi for the

purchase of ESI mass spectrometer through FIST grant is also gratefully acknowledged.

References

1. B. O'Regan, M. Grätzel, Nature **353**, 737–740 (1991)
2. M. Grätzel, J. Photochem. Photobiol. C **4**, 145–153 (2003)
3. Z. Ning, Y. Fu, H. Tian, Energy. Environ. Sci. **3**, 1170–1181 (2010)
4. C. Grätzel, S.M. Zakeeruddin, Mater. Today **16**, 11–18 (2013)
5. J.-Q. Jiang, C.-L. Sun, Z.-F. Shi, H.-L. Zhang, RSC Adv. **4**, 32987–32996 (2014)
6. C.-P. Lee, R.Y.-Y. Lin, L.-Y. Lin, C.-T. Li, T.-C. Chu, S.-S. Sun, J.T. Lin, K.-C. Ho, RSC Adv. **5**, 23810–23825 (2015)
7. G. Chen, H. Sasabe, T. Igarashi, Z. Hong, J. Kido, J. Mater. Chem. A **3**, 14517–1453 (2015)
8. S. Mathew, A. Yella, P. Gao, R. Humphry-Baker, B.F. Curchod, N. Ashari-Astani, I. Tavernelli, U. Rothlisberger, M.K. Nazeeruddin, M. Grätzel, Nat. Chem. **6**, 242–247 (2014)
9. C.-Y. Chen, M. Wang, J.-Y. Li, N. Pootrakulchote, L. Alibabaei, C.-H. Ngoc-le, J.-D. Decoppet, J.-H. Tsai, C. Grätzel, C.-G. Wu, S.M. Zakeeruddin, M. Grätzel, ACS Nano **3**, 3103–3109 (2009)
10. Z. Yao, M. Zhang, H. Wu, L. Yang, R. Li, P. Wang, J. Am. Chem. Soc. **137**, 3799–3808 (2015)
11. A. Hagfeldt, G. Boschloo, L. Sun, L. Kloo, H. Pettersson, Chem. Rev. **110**, 6595–6663 (2010)
12. A. Mishra, M.K.R. Fischer, P. Bäuerle, Angew. Chem. Int. Ed. **48**, 2474–2499 (2009)
13. M. Liang, J. Chen, Chem. Soc. Rev. **42**, 3453–3488 (2013)
14. W.H. Zhu, Y.Z. Wu, S.T. Wang, W.Q. Li, X. Li, J. Chen, Z.S. Wang, H. Tian, Adv. Funct. Mater. **21**, 756–763 (2011)
15. Y. Wu, W. Zhu, Chem. Soc. Rev. **42**, 2039–2058 (2013)
16. Y. Wu, W.-H. Zhu, S.M. Zakeeruddin, M. Grätzel, ACS Appl. Mater. Interfaces **7**, 9307–9318 (2015)
17. Y.Z. Wu, M. Marszalek, S.M. Zakeeruddin, Q. Zhang, H. Tian, M. Grätzel, W.H. Zhu, Energy Environ. Sci. **5**, 8261–8272 (2012)
18. H.B. Zhu, W.Q. Li, Y.Z. Wu, B. Liu, S.Q. Zhu, X. Li, H. Ågren, W.H. Zhu, ACS Sustain. Chem. Eng. **2**, 1026–1034 (2014)
19. Z. Yao, M. Zhang, R. Li, L. Yang, Y. Qiao, P. Wang, Angew. Chem. Int. Ed. **54**, 5994–6008 (2015)
20. J. Mao, F. Guo, W. Ying, W. Wu, J. Li, J. Hua, Chem. Asian J. **7**, 982 (2012)
21. Y. Yen, C. Lee, C. Hsu, H. Chou, Y. Chen, J.T. Lin, Chem. Asian J. **8**, 809–816 (2013)
22. J.-S. Ni, Y.-C. Yen, J.T. Lin, Chem. Commun. **51**, 17080–17083 (2015)
23. J. Yang, P. Ganesan, J. Teuscher, T. Moehl, Y.J. Kim, C. Yi, P. Comte, K. Pei, T.W. Holcombe, M.K. Nazeeruddin, J. Hua, S.M. Zakeeruddin, H. Tian, M. Grätzel, J. Am. Chem. Soc. **136**, 5722–5730 (2014)
24. X. Li, Y. Hu, I. Sanchez-Molina, Y. Zhou, F. Yu, S.A. Haque, W. Wu, J. Hua, H. Tiana, N. Robertson, J. Mater. Chem. A **3**, 21733–21743 (2015)
25. S.Y. Qu, C. Qin, A. Islam, Y.Z. Wu, W.H. Zhu, J.L. Hua, H. Tian, L.Y. Han, Chem. Commun. **48**, 6972–6974 (2012)
26. S.S. Li, K.-J. Jiang, F. Zhang, J.-H. Huang, S.-G. Li, M.-G. Chen, L.-M. Yang, Y.-L. Song, Org. Electron. **15**, 1579–1585 (2014)
27. H. Li, Y. Wu, Z. Geng, J. Liu, D. Xu, W. Zhu, J. Mater. Chem. A **2**, 14649–14657 (2014)
28. H. Zhu, Y. Wu, J. Liu, W. Zhang, W. Wu, W.-H. Zhu, J. Mater. Chem. A **3**, 10603–10609 (2015)
29. K. Kakiage, Y. Aoyama, T. Yano, T. Otsuka, T. Kyomen, M. Unnoc, M. Hanaya, Chem. Commun. **50**, 6379–6381 (**2014**)
30. L.-L. Tan, J.-F. Huang, Y. Shen, L.-M. Xiao, J.-M. Liu, D.-B. Kuanga, C.-Y. Su, J. Mater. Chem. A **2**, 8988–8994 (2014)
31. S.S. Soni, K.B. Fadadu, J.V. Vaghasiya, B.G. Solanki, K.K. Sonigara, A. Singh, D. Das, P.K. Iyer, J. Mater. Chem. A **3**, 21664–21671 (2015)
32. X. Qian, Y.-Z. Zhu, W.-Y. Chang, J. Song, B. Pan, L. Lu, H.-H. Gao, J.-Y. Zheng, ACS Appl. Mater. Interfaces **7**, 9015–9022 (2015)
33. X. Yang, J. Zhao, L. Wang, J. Tiana, L. Suna, RSC Adv. **4**, 24377–24383 (2014)
34. M. Mao, X.-L. Zhang, X.-Q. Fang, G.-H. Wu, S.-Y. Dai, Q.-H. Song, X.-X. Zhang, J. Power Sources **268**, 965–976 (2014)
35. A. Baheti, K.R.J. Thomas, C.-T. Li, C.-P. Lee, K.-C. Ho, ACS Appl. Mater. Interfaces **7**, 2249–2262 (2015)
36. Z. Iqbal, W.-Q. Wu, Z.-S. Huang, L. Wang, D.-B. Kuang, H. Meier, D. Cao, Dyes Pigm. **124**, 63–71 (2016)
37. H. Lee, S.B. Yuk, J. Choi, H.J. Kim, H.W. Kim, S.H. Kim, B. Kim, M.J. Ko, J.P. Kim, Dyes Pigm. **102**, 13–21 (2014)
38. J. Li, X. Yang, M. Cheng, M. Wang, L. Sun, Dyes Pigm. **116**, 58–64 (2015)
39. Y.-F. Chen, J.-M. Liu, J.-F. Huang, L.-L. Tan, Y. Shen, L.-M. Xiao, D.-B. Kuang, C.-Y. Su, J. Mater. Chem. A **3**, 8083–8090 (2015)
40. K. Ogawa, S.C. Rasmussen, J. Org. Chem. **68**, 2921–2928 (2003)
41. S.C. Rasmussen, S.J. Evenson, Prog. Polym. Sci. **38**, 1773–1804 (2013)
42. J. Zhang, Z. Yao, Y. Cai, L. Yang, M. Xu, R. Li, M. Zhang, X. Donga, P. Wang, Energy Environ. Sci. **6**, 1604–1614 (2013)
43. N. Cai, J. Zhang, M. Xu, M. Zhang, P. Wang, Adv. Funct. Mater. **23**, 3539–3547 (2013)
44. Z. Wang, M. Liang, L. Wang, Y. Hao, C. Wang, Z. Sun, S. Xue, Chem. Commun. **49**, 5748–5750 (2013)
45. Z. Wang, H. Wang, M. Liang, Y. Tan, F. Cheng, Z. Sun, ACS Appl. Mater. Interfaces **6**, 5768–5778 (2014)
46. Z. Wang, M. Liang, Y. Tan, L. Ouyang, Z. Suna, S. Xue, J. Mater. Chem. A **3**, 4865–4874 (2015)
47. S. Kumar, K.R.J. Thomas, C.-T. Li, K.-C. Ho, Org. Electron. **26**, 109–116 (2015)
48. Y. Xie, W. Wu, H. Zhu, J. Liu, W. Zhang, H. Tian, W.-H. Zhu, Chem. Sci. **7**, 544–549 (2016)
49. D. Sahu, H. Padhy, D. Patra, J.-F. Yin, Y.-C. Hsu, J.-T. Lin, K.-L. Lu, K.-H. Wei, H.-C. Lin, Tetrahedron **67**, 303–311 (2011)
50. P. Dai, L. Yang, M. Liang, H. Dong, P. Wang, C. Zhang, Z. Sun, S. Xue, ACS Appl. Mater. Interfaces **7**, 22436–22447 (2015)
51. N. Miyaura, A. Suzuki, Chem. Rev. **95**, 2457–2483 (1995)
52. J.K. Stille, Angew. Chem. Int. Ed. **25**, 508–524 (1986)
53. E. Knoevenagel, Chem. Ber. **29**, 172 (1896)
54. J. Liu, R. Zhang, G. Sauvé, T. Kowalewski, R.D. McCullough, J. Am. Chem. Soc. **130**, 13167–13176 (2008)
55. D.G.D. Patel, F. Feng, Y. Ohnishi, K.A. Abboud, S. Hirata, K.S. Schanze, J. Am. Chem. Soc. **134**, 2599–2612 (2012)
56. C. Reichardt, Chem. Rev. **94**, 2319–2358 (1994)
57. A. Granzhan, H. Ihmels, G. Viola, J. Am. Chem. Soc. **129**, 1254–1267 (2007)
58. K. Sayama, S. Tsukagoshi, K. Hara, Y. Ohga, A. Shinpou, Y. Abe, S. Suga, H. Arakawa, J. Phys. Chem. B **106**, 1363–1371 (2002)
59. H. Raghuraman, D.A. Kelkar, A. Chattopadhyay, in *Reviews in Fluorescence 2005*, ed. by C.D. Geddes, J. R. Lakowicz (Springer, New York, 2005), p. 199
60. N. Blouin, A. Michaud, D. Gendron, S. Wakim, E. Blair, R. Neagu-Plesu, M. Belletete, G. Durocher, Y. Tao, M. Leclerc, J. Am. Chem. Soc. **130**, 732–742 (2007)
61. M. Grätzel, Nature **414**, 338–344 (2001)

62. A.N.M. Green, E. Palomares, S.A. Haque, J.M. Kroon, J.R. Durrant, J. Phys. Chem. B **109**, 12525–12533 (2005)
63. D. Sholl, J.A. Steckel, *Density Functional Theory: A Practical Introduction* (Wiley-VCH, Somerset, 2009)
64. W. Koch, M.C. Holthausen, *A Chemist's Guide to Density Functional Theory* (Wiley-VCH, Weinheim, 2000)
65. S.-Q. Fan, Y. Geng, C. Kim, S. Paik, J. Ko, Mater. Chem. Phys. **132**, 943–949 (2012)
66. J.-H. Yum, S.R. Jang, R. Humphry-Baker, M. Grätzel, J.-J. Cid, T. Torres, M.K. Nazeeruddin, Langmuir **24**, 5636–5640 (2008)
67. P. Bonhôte, J.-E. ; Moser, R. Humphry-Baker, N. Vlachopoulos, S.M. Zakeeruddin, L. Walde, M. Grätzel, J. Am. Chem. Soc. **121**, 1324–1336 (1999)
68. W. Ying, F. Guo, J. Li, Q. Zhang, W. Wu, H. Tian, J. Hua, ACS Appl. Mater. Interfaces **4**, 4215–4224 (2012)
69. S. Qu, B. Wang, F. Guo, J. Li, W. Wu, C. Kong, Y. Long, J. Hua, Dyes Pigm. **92**, 1384–1393 (2012)
70. I. Mora-Seró, S. Giménez, F. Fabregat-Santiago, R. Gòmez, Q. Shen, T. Toyoda, Acc. Chem. Res. **42**, 1848–1857 (2009)
71. J. Van de Lagemaat, N.-G. Park, A.J. Frank, J. Phys. Chem. B **104**, 2044–2052 (2000)